Comprehensive histological imaging of native microbiota in human glioma

Jiajia Zhao
Zhujiang Hospital, Southern Medical University
Dian He
Zhujiang Hospital, Southern Medical University
Hei Ming Lai
Department of Psychiatry, Faculty of Medicine, The Chinese University of Hong Kong
Yingying Xu
School of Biomedical Engineering and Guangdong Provincial Key Laboratory of Medical Image Processing, Southern Medical University
Yunhao Luo
Zhujiang Hospital, Southern Medical University
Ting Li
Zhujiang Hospital, Southern Medical University
Jianhao Liang
Zhujiang Hospital, Southern Medical University
Xiaodu Yang
School of Biomedical Engineering and Guangdong Provincial Key Laboratory of Medical Image Processing, Southern Medical University
Linlang Guo
Zhujiang Hospital, Southern Medical University
Yiquan Ke
Zhujiang Hospital, Southern Medical University
Hongwei Zhou
Zhujiang Hospital, Southern Medical University
Wu-Tian Wu
Guangdong-Hong Kong-Macau Institute of CNS Regeneration (GHMICR), Jinan University
Hongbo Guo
Zhujiang Hospital, Southern Medical University
Haitao Sun (2009sht@smu.edu.cn)
Southern Medical University

Article

Keywords: Glioma, Microbiota, Tissue clearing, Fluorescent labeling, Three-dimensional visualization, Image processing

Posted Date: July 31st, 2021

DOI: https://doi.org/10.21203/rs.3.rs-755297/v1

Version of Record: A version of this preprint was published at Journal of Biophotonics on December 22nd, 2021. See the published version at https://doi.org/10.1002/jbio.202100351.

Comprehensive histological imaging of native microbiota in human glioma

Jiajia Zhao[1,2#], Dian He[2#], Hei Ming Lai[3], Yingying Xu[4], Yunhao Luo[1], Ting Li[2], Jianhao Liang[2], Xiaodu Yang[4], Linlang Guo[5], Yiquan Ke[2], Hongwei Zhou[1], Wutian Wu[6,7*], Hongbo Guo[2*], Haitao Sun[1, 2, 8*]

[1] Microbiome Medicine Center, Clinical Biobank Center, Department of Laboratory Medicine, Zhujiang Hospital, Southern Medical University, Guangzhou 510280, China

[2] Neurosurgery Center, The National Key Clinical Specialty, The Engineering Technology Research Center of Education Ministry of China on Diagnosis and Treatment of Cerebrovascular Disease, Guangdong Provincial Key Laboratory on Brain Function Repair and Regeneration, The Neurosurgery Institute of Guangdong Province, Zhujiang Hospital, Southern Medical University, Guangzhou 510280, China

[3] Department of Psychiatry, Faculty of Medicine, The Chinese University of Hong Kong, Shatin, Hong Kong.

[4] School of Biomedical Engineering and Guangdong Provincial Key Laboratory of Medical Image Processing, Southern Medical University, Guangzhou, 510515, China.

[5] Department of Pathology, Zhujiang Hospital, Southern Medical University, 510280, Guangzhou, China.

[6] *Guangdong-Hong Kong-Macau Institute of CNS Regeneration (GHMICR), Jinan University*, Guangzhou 510632, China

[7] Re-Stem Biotechnology Co., Ltd, Suzhou, 215300, China

[8] Key Laboratory of Mental Health of the Ministry of Education, Guangdong–Hong Kong–Macao Greater Bay Area Center for Brain Science and Brain-Inspired Intelligence, Southern Medical University, Guangzhou 510515, China

[#] Contributed equally.

[*] **Corresponding authors:**

Haitao Sun, E-mail: 2009sht@smu.edu.cn; ORCID: 0000-0001-7925-9506

Hongbo Guo, E-mail: guohongbo911@126.com;

Wutian Wu, E-mail:wtwu@hku.hk;

Abstract:

Mounting evidence suggests that distinct microbial communities reside in tumors and play important roles in tumor physiology. Recently, Nejman et al. profiled the composition and localization of intratumoral bacteria using 16S DNA sequencing and histological visualization methods across seven tumor types, including human glioblastoma. However, considering potential contamination in their sample origins and processing, the results based on traditional histological methods need to be validated. Here, we propose a three-dimensional (3D) intratumoral microbiota visualization and quantification protocol to observe microbiota in intact tumor tissues on the premise of avoiding possible contamination in the surface of tissues, based on tissue clearing, immunofluorescent labeling, microscopy imaging, and image processing. For the first time, we have achieved 3D quantitative imaging of bacterial LPS fluorescent signals deep in gliomas in a contamination-free manner, which was founded mostly localized near nuclear membranes or in the intercellular space. Through an automated statistical algorithm, reliable signals can be distinguished for further analysis of their sizes, distribution, and fluorescence intensities. Combining two-dimensional images from multiple thin-section histological methods, including immunochemistry and fluorescence in situ hybridization, we provide a comprehensive histological investigation of the morphology and distribution of these signals on human glioma samples. We expect that this multi-evidence chain will provide supporting proof for the presence of intratumoral bacteria in human glioma and that the integrated pipeline can be applied to investigate the native bacteria within diverse tumors and contribute to the interpretation of their direct roles in the tumor microenvironment.

Keywords:

Glioma; Microbiota; Tissue clearing; Fluorescent labeling; Three-dimensional visualization; Image processing

Introduction:

Ever-increasing evidence has shown that the native microbiota constitutes an essential component of the tumor microenvironment across many tumor types[1-3]. The populations of bacteria colonized within tumors have been demonstrated to be tumor-type specific, which may directly regulate cancer initiation, progression, and patients' responses to therapies[1, 3, 4]. Glioma is the most common primary brain cancer and glioblastoma (GBM) is the most malignant kind with a poor prognosis and remains incurable[5]. Recently, Nejman et al. verified that bacteria exist within seven tumors, including brain tumors, via combinational methods of immunohistochemistry, fluorescence *in situ* hybridization (FISH), electron microscopy (EM), culturomics, and genomic sequencing[4]. Nonetheless, their conclusions, despite their strict protocol of DNA sequencing against contamination, need to be further validated in consideration of potential contamination that can be traced back to sample resources and experimental procedures, especially when histological methods are involved. Meanwhile, these methods may lead to misinterpretation of the quantification and biogeography of microbial communities due to the lack of spatial resolution (e.g., thin sections) or individual-cell information (e.g., bulk sequencing for cell population).

To detect the presence, localization, and morphology of intratumoral bacteria, histological methods relied on ultra-thin or thin tissue sections play a pivotal role, whereas often fail to avoid possible contamination on the surface of tissue sections and greatly restrict the information content. Regarding these defects, the novel tissue clearing techniques are expected to provide a contamination-free manner of microbial detection for tumor samples via direct interrogation of intact tissues[6, 7]. By providing the quantitative *in-situ* three-dimensional (3D) information of intratumoral microbiota in single-cell resolution, the tissue clearing-based visualization approach will promise to help validate the presence of residing microbial communities within the tumor and interpret their role from a system biological perspective. Here we undertook a comprehensive study on bacterial components within human gliomas combining 3D

visualization of intact tissues and traditional histological staining of formalin-fixed, paraffin-embedded (FFPE) slices. We provided the first 3D, quantitative, and contamination-free information of bacterial LPS fluorescent signals within human gliomas via the proposed tissue clearing-based intratumoral microbiota imaging strategy. Combining these pieces of histological evidence, we hope to give support to the presence of bacteria in gliomas and contribute to a comprehensive analysis in regards to their sizes, morphologies, and spatial distributions. Incorporating more methodologic improvements, this 3D *in situ* quantitative intratumoral microbiota imaging strategy is promising to reveal the panorama of the human glioma microbiota and is expected to provide insightful information into the direct host-microbiota interactions in the glioma microenvironment soon.

Results

3D quantitative imaging of bacterial LPS fluorescent signals in human glioma samples

To eliminate the negative impacts of potential contamination during the tissue sampling and handling of tumor tissues for intratumor microbiota detection, we developed an Accu-Opticlear-based tissue clearing protocol to observe microbes within tissues, and for the first time, accomplished 3D visualization of bacterial LPS fluorescent signals in human glioma samples (**Fig.1** a-c). We used antibodies to target the LPS cores anchored in the cell wall of Gram-negative bacteria and verified their specificity (**Extended Data Fig.1** a-b), which also had been well validated by Nejman et al. examining human tumor tissue microarrays over seven tumor types[4]. Here, the human glioma samples were sliced into 500 μm-thick sections and cleared by the Accu-Opticlear protocol in combination with an autofluorescence bleaching step in clean environments with sterilized reagents and equipment. The most superficial parts, around 50-100 μm, were ignored during imaging by multiphoton laser scanning microscopy (MPLSM), and an

internal 100 μm part was scanned at a light-cutting interval of 1 μm **(Fig.1** a-c**)**. The 3D reconstruction images and videos clearly showed the sporadic distribution and irregular shapes of LPS fluorescent signals, which were mostly located near the nuclear membranes or diffused in intercellular spaces **(Fig.1** d**; Supplementary Movie S1**; **Supplementary Movie S2**)**.** We provided an automated image processing pipeline to exclude fluorescent signals with improper sizes and allow quantitative analysis in terms of the load, size, and fluorescent intensity of the signals (**Fig.1** e; **Extended Data Fig.1** c-e). Quantitative analysis also suggested that these signals were randomly localized and of uneven sizes, with an average diameter of 2.17±0.80 μm. Whereas the low sample amount and microscopic fields in this study limited a thorough investigation of the universal features and distribution patterns of bacterial LPS in gliomas. In addition, these LPS fluorescent signals within glioma exhibited neither the typical features nor complete profiles of Gram-negative bacteria, which possibly attributes to the deficiency of cell walls and envelope transformation of intracellular bacteria[4]. Also, steps such as formalin fixation and permeation can alter bacterial morphology and introduce artifacts[8] (**Extended Data Fig.1** b).

Taken together, despite further requirements for methodological improvements, this 3D quantitative *in situ* intratumoral bacteria imaging method provides the first direct and contaminant-free image of bacterial LPS fluorescent signals within human glioma samples. We also developed a customized statistical algorithm to accurately capture LPS fluorescent signals and give a quantitative description of their morphology and distribution. This integrated protocol for detecting and analyzing intratumoral bacterial components is also applicable to the investigation of diverse tumors and promises to advance the direct study of host-microbe interactions.

Bacterial LPS and RNA can be visualized in human glioma samples

To further complement the acquired 3D information, we performed traditional histopathological examinations for tissues from the same samples. We adopted antibodies against bacterial LPS and lipoteichoic acid (LTA) to target Gram-negative

and Gram-positive bacteria via immunohistochemistry staining, respectively. We demonstrated similar results as Rejman et al. reported[4], that LPS was detected in glioma samples while LTA was absent (**Fig. 2**). Universal 16S rRNA FISH probes were applied to detect bacteria, with antisense probes serving as control. Distinct localization of bacterial 16S rRNA signals was founded mostly alongside the nuclear membrane, irregular in shape (**Fig. 3**). Quantification of fluorescent signals showed sizes ranging from 0.26~4.26 μm, with an average diameter of 0.59~1.85 μm. The results of 16S rRNA FISH staining combined with those of bacterial LPS immunostaining further indicated the atypical and variable morphologies of these bacterial components in tumor tissues. Although the two-dimensional (2D) images lacked vertical spatial information, these pieces of evidence were in support of the discoveries in 3D and added to the proof of the presence of bacteria in human gliomas.

Discussion

In the present work, we combined multiple histological methods to investigate bacteria in human glioma samples. We developed an Accu-OptiClearing-based contaminant-free 3D pathology protocol to image bacterial components in human glioma, allowing further analysis for their quantification and distribution characteristics. This 3D histology imaging protocol is optimized by 1) collecting, sectioning, and processing the sample in clean environments and using sterilized reagents and equipment; 2) including negative and positive controls to monitor contamination and determine the effectiveness of the results; 3) studying the inside rather than the surface of intact cleared samples; 4) quenching autofluorescence to eliminate interference from unwanted fluorescent signals. We also represented, to our best knowledge, the first attempt to visualize and measure the bacterial LPS fluorescent signals *in situ* in the context of 3D histology free of contamination. This protocol also gives wide access to the visualization and quantification of bacterial signals within diverse tumors, aiming to provide a systematic characterization of the distribution and morphologies of intratumoral bacteria *in situ*. Besides, we built the multi-evidence chain that combines 2D and 3D histology to

comprehensively investigate these signals within human glioma, which will help verify the existence of intratumoral bacteria in human glioma.

Although we have optimized the 3D imaging protocol to exclude potential contamination, there remain possible impacts of postmortem microbial translocation and other unaware contaminants, a universal problem in examining postmortem samples. Procedures such as shortening postmortem intervals, including sterile operations, and coupling with negative controls can help reduce errors[9]. Better approaches may be to identify microbes in fresh tumor tissues by vitro culture method and even directly track microbes *in vivo*. Immunofluorescent labeling for thick tissues raises recurring difficulties in eradicating non-specific fluorescence from non-specific binding of antibodies and autofluorescence derived to natural pigments (e.g., lipofuscin, flavin, mitochondria, hemoglobin, etc.) or formalin fixation. Autofluorescence in biological tissues, unfortunately, exhibits broad spectral ranges of excitation and emission wavelengths and approximate features similar to bacterial fluorescence profiles[10-12]. A preference for long-wavelengths fluorophores is recommended since the typical autofluorescence is mostly overlapped with green-blue fluorophores. Studies report that $CuSO_4$ and SBB stains unwanted autofluorescence black, such as lipofuscin, an aging-related pigment that accumulates in many cells including those of the central nervous system, via boundary surface adsorption[11, 13]. To minimize the interference of autofluorescence, here we used chemicals ($CuSO_4$ and SBB)[13] to mask autofluorescence while enabling maintenance of tissue transparency and specific fluorescent labels. Facilitated by computing algorithms, fluorescence thresholding can also be automatically performed. However, both approaches have drawbacks, such as chemical quenching may reduce immunolabeling and the accuracy of automated spectral thresholding is unstable[13]. The protocol also needs to be reassessed whenever an experiment element is adjusted, to produce the most biologically relevant results. Problems also arise in the accuracy and sensitivity of 3D quantitative analysis for the signals, considering tissue deformation (e.g., shrinkage and expansion) and

immunofluorescence inaccessibility to all the targets during tissue clearing, which may ultimately derive to inaccurate parameters (e.g., diameter and quantity, etc.)[14]. Meanwhile, the confined sample size and microscopic fields of this study reduced the validity of the analysis. As a preliminary study, the incomplete nature of this work limited the information we acquired and prevented us from interpreting the constitution and roles of intratumoral bacteria. We hope to increase the reliability of fluorescent labeling for bacteria in tissue sections and 3D quantitative analysis in future research, and explore the underlying molecular mechanisms. This work also highlights the dilemma in histological detection of intratumoral microbiota, where results from multiple methods should be combined to make a comprehensive judgment.

While the present study adds to the picture of the glioma microbiota，more issues warrant further investigation. The tumor-specific composition and function of the tumor microbiome have been the upsurge of omics sequencing and clustering analysis[15-17]. For the brain, the organ thought to be distinctively immune-privileged against microbial invasion by physiological barriers (e.g., blood-brain barrier (BBB)), how microbiota evolves and resides in brain tumors post an interesting question. Robert et al. once reported finding rod-shaped bacteria in healthy human postmortem brains by EM and proposed that bacteria may enter the brain through the BBB or via nerves innervating the gut, however, lacking further verification[18]. Although the bidirectional “gut-brain axis” has been defined to describe the interaction of the gut microbiome and the brain, only indirect pathways have been confirmed so far[3, 19-21]. While most studies on the direct host-bacteria interaction focused on how local microbial communities affect colonized tumors, yet remaining little is known[22]. Driven by the advances in bacterial probing and characterization, such as the development of STAMP[23] and HIPR-FISH[24] techniques, tissue clearing technology is expected to be armed as a powerful tool in profiling the human tumor microbiota. We expect that 3D *in-situ* quantitative imaging of intratumoral microbiota in their native context with single-cell resolution will promote the dissection of the intricate interactive network among microbiota, tumor

cells, immune cells, and other components in the tumor microenvironment.

Reference

1. Sepich-Poore, G.D. *et al.* The microbiome and human cancer. *Science* **371**, eabc4552 (2021).
2. Helmink, B.A., Khan, M.A.W., Hermann, A., Gopalakrishnan, V. & Wargo, J.A. The microbiome, cancer, and cancer therapy. *Nat Med* **25**, 377-388 (2019).
3. Xavier, J.B. *et al.* The Cancer Microbiome: Distinguishing Direct and Indirect Effects Requires a Systemic View. *Trends Cancer* **6**, 192-204 (2020).
4. Nejman, D. *et al.* The human tumor microbiome is composed of tumor type-specific intracellular bacteria. *Science* **368**, 973-980 (2020).
5. Tan, A.C. *et al.* Management of glioblastoma: State of the art and future directions. *CA Cancer J Clin* **70**, 299-312 (2020).
6. Ueda, H.R. *et al.* Whole-Brain Profiling of Cells and Circuits in Mammals by Tissue Clearing and Light-Sheet Microscopy. *Neuron* **106**, 369-387 (2020).
7. Ueda, H.R. *et al.* Tissue clearing and its applications in neuroscience. *Nat Rev Neurosci* **21**, 61-79 (2020).
8. Park, S., Reyer, M.A., McLean, E.L., Liu, W. & Fei, J. An Improved Method for Bacterial Immunofluorescence Staining To Eliminate Antibody Exclusion from the Fixed Nucleoid. *Biochemistry* **58**, 4457-4465 (2019).
9. Zhan, X. *et al.* Gram-negative bacterial molecules associate with Alzheimer disease pathology. *Neurology* **87**, 2324-2332 (2016).
10. Croce, A.C. & Bottiroli, G. Autofluorescence spectroscopy and imaging: a tool for biomedical research and diagnosis. *Eur J Histochem* **58**, 2461 (2014).
11. Schnell, S.A., Staines, W.A. & Wessendorf, M.W. Reduction of Lipofuscin-like Autofluorescence in Fluorescently. *J Histochem Cytochem* **47**, 719-730 (1999).
12. Lee, T.B., Lee, J. & Jun, J.H. Three-Dimensional Approaches in Histopathological Tissue Clearing System. *The Korean Journal of Clinical Laboratory Science* **52**, 1-17 (2020).
13. Jenvey, C.J. & Stabel, J.R. Autofluorescence and Nonspecific Immunofluorescent Labeling in Frozen Bovine Intestinal Tissue Sections: Solutions for Multicolor Immunofluorescence Experiments. *J Histochem Cytochem* **65**, 531-541 (2017).
14. Francis, R.J. *et al.* Three-dimensional in situ morphometrics of Mycobacterium tuberculosis infection within lesions by optical mesoscopy and novel acid-fast staining. *Sci Rep* **10**, 21774 (2020).
15. Livyatan, I., Nejman, D., Shental, N. & Straussman, R. Characterization of the human tumor microbiome reveals tumor-type specific intra-cellular bacteria. *Oncoimmunology* **9**, 1800957 (2020).
16. Riquelme, E. *et al.* Tumor Microbiome Diversity and Composition Influence Pancreatic Cancer Outcomes. *Cell* **178**, 795-806 e712 (2019).
17. Thyagarajan, S. *et al.* Comparative analysis of racial differences in breast tumor microbiome. *Sci Rep* **10**, 14116 (2020).
18. Roberts R C, F.C.B., Walker C K. The human brain microbiome; there are bacteria in our

brains! . *In: Neuroscience Meeting Planner. SanDiego, CA: Society for Neuroscience* (2018).
19. Mehrian-Shai, R., Reichardt, J.K.V., Harris, C.C. & Toren, A. The Gut-Brain Axis, Paving the Way to Brain Cancer. *Trends Cancer* **5**, 200-207 (2019).
20. Fung, T.C. The microbiota-immune axis as a central mediator of gut-brain communication. *Neurobiol Dis* **136**, 104714 (2020).
21. Lyu, Y., Yang, H. & Chen, L. Metabolic regulation on the immune environment of glioma through gut microbiota. *Semin Cancer Biol* **S1044-579X(21)00133-4** (2021).
22. Zhao, K. & Hu, Y. Microbiome harbored within tumors: a new chance to revisit our understanding of cancer pathogenesis and treatment. *Signal Transduct Target Ther* **5**, 136 (2020).
23. Wang, W. *et al.* Assessing the viability of transplanted gut microbiota by sequential tagging with D-amino acid-based metabolic probes. *Nat Commun* **10**, 1317 (2019).
24. Shi, H. *et al.* Highly multiplexed spatial mapping of microbial communities. *Nature* **588**, 676-681 (2020).

Methods

Human glioma samples

3 human glioma samples used in this study were randomly selected and obtained during neurosurgeries at the Zhujiang Hospital (Supplementary Table 1, Online Resource 1). Informed consent has been obtained for utilizing the resected tissues for research, with prior approval by the Medical Ethics Committee of Zhujiang Hospital of Southern Medical University (Approval Number: 2018-SJWK-004 and 2020-YBK-001-02). The specimens were resected and immediately fixed in neutral buffered formalin (NBF) and sent for diagnostic pathological examination. Tissues not used in the clinical-pathological examination were salvaged for this study. These consisted of fragmented pieces of brain tumors, which have not been embedded in paraffin wax. The total duration of tissue fixation in NBF was about 9 to 11 months at 4˚C. The 3 samples were diagnosed by clinicians and graded according to WHO classification.

Animals

C57BL/6 mice (8-9 weeks old, 18-22 g, male) were obtained and raised in the Experimental Animal Center of Zhujiang Hospital of Southern Medical University, Zhujiang Hospital, and fed in a specific pathogen-free lab with constant temperature and humidity. The cage, pad, feed, etc., were sterilized by high-pressure steam and

replaced regularly. All animal experiments in this study were performed in strict compliance with the ethical principles of experimental animal welfare.

Mouse dissection and organ collection

A C57BL/6 mouse was deeply anesthetized with 1% pentobarbital sodium. The mouse was perfused with saline, followed by 4% (w/v) paraformaldehyde (PFA) fixation. The total intestinal tract was dissected separately and rinsed with 4% PFA to remove intestinal contents. The sample was post-fixed in 4% PFA for 2 days at 4˚C. Another C57BL/6 mouse was killed by neck-breaking and the brain was dissected and immediately collected. The brains were post-fixed with 4% PFA at 4˚C for 3 days. Before tissue clearing, tissues were gently rinsed with 0.01% (w/v) phosphate-buffer saline (1×PBS) twice.

Bacteria smear and immunolabeling

The preparation of bacteria smears and immunolabeling were followed the literiture[25]. A loopful of gram-negative bacteria (Escherichia coli strain ATCC25922) cultured in a Columbia agar base (Guangzhou Dijing Microbial Technology Co., Ltd. #LS0109) were transferred to clean EP tubes and fixed in PFA for 1 day. EP tubes were centrifuged (15 minutes, 4000-8000×g, at 4˚C) and the supernatant was removed. The bacteria pellet was resuspended in PBS and washed 3 times. A loopful of the resuspended bacteria was transferred into a drop of ddH_2O in the center of clean slides to make a suspension, air-dried. The smears were fixed in 95% (v/v) ethanol for 1 minute at RT and dipped in PBS, air-dried. Immunolabeling of bacteria was performed according to the standard staining method. Primary antibodies (Lipopolysaccharide Core, mAb WN1 222-5, HycultBiotech #HM6011, 1:100 dilution) were applied on smears for 30 minutes at 37˚C and secondary antibodies (Donkey anti-Mouse IgG (H+L) Highly Cross-Adsorbed Secondary Antibody, Alexa Fluor Plus 594, Thermo Fisher #A32744, 1:100 dilution) were added for 30 minutes at 37˚C. The slides were rinsed in PBS for 30 minutes at RT and then blotted with Kimwipe paper. The slides were mounted with

mounting medium with 4',6-diamidino-2-phenylindole (DAPI) (Fluoroshield Mounting Medium With DAPI, ABCAM #ab104139) and coverslips to the smears. The slides were observed with confocal laser scanning microscopy (LSM 800, Carl Zeiss, Germany) equipped with the objectives Plan-Apochromat 63X/1.40 Oil DIC M27.

Immunofluorescence labeling and tissue clearing

Before immunolabeling and tissue clearing, samples were trimmed and sectioned with vibrating slicers (DOSAKA, DTK-2ER01N) into 500 μm-thick slices. Accu-OPTIClearing and reagent preparation were modified according to the literature[26]. Autofluorescence quenching chemicals were prepared according to the literature[27]：10 mM Cupric sulfate ($CuSO_4$, MACLIN #C805782) in 50 mM ammonium acetate buffer (adjust the pH = 5.0); 1% Sudan Black B (SBB, Solarbio #S8300) in 70% ethanol (protect from light). Sections were incubated in either 1×PBS (control), 10 mM $CuSO_4$, or 1% SBB for 2 hours at RT with shaking. Sections were then dipped in ddH_2O and rinsed in 1×PBS. Sections were cleared with Accu-OPTIClearing solution (4% SDS-OPTIClear incubation at 37˚C) for 2 days and then washed with 1×PBS (3×10 minutes) at RT. Sections were then blocked with blocking buffer (0.6 M glycine, 0.2% v/v Triton X-100, 3% v/v donkey serum, with 0.01% w/v sodium azide in 1× PBS) overnight at 37˚C. Sections were incubated with primary antibodies (Lipopolysaccharide Core, mAb WN1 222-5, HycultBiotech #HM6011, 1:100 dilution) in antibody diluent (PBS buffer, containing 0.2% v/v Tween 20, 3% donkey serum，0.01% sodium azide) at 37˚C for 2 days. Primary antibodies were removed by washing with 0.2% PBS-Tween 20 (6×30 minutes) at RT on a shaker and then left overnight. Sections were incubated with secondary antibodies (Donkey anti-Mouse IgG (H+L) Highly Cross-Adsorbed Secondary Antibody, Alexa Fluor Plus 594, Thermo Fisher #A32744, 1:100 dilution) overnight, protected from light. Sections were counterstained with 1 μg/ml DAPI during secondary antibody staining. After washing off secondary antibodies with 0.2% PBS-Tween 20 (6×30 minutes, at RT) on a shaker, sections were incubated with OPTIClear solution for 15 hours before microscopy. All solutions were sterilized with

0.22 μm filters (MILLEX-GV, SLGV033RS) and the operations were carried out in a biosafety cabinet (Thermo Fisher #1374-M) after UV disinfection. Gently transfer the sample to avoid damage.

Multiphoton laser scanning microscopy (MPLSM) imaging

All cleared tissues were mounted on 60 mm cell and tissue culture dishes wetted with OPTIClear solution (about 200 μl) under the microscopy. Images were obtained with an MPLSM (Olympus, FVMPE-RS, Tokyo, Japan) equipped with XLPLN10XSVMP (×10/0.6 NA) objective lens. We determined the optimal excitation wavelength of fluorescent dyes by gradually adjusting the wavelength of excitation light from 680 nm to 1050 nm. The excitation laser wavelengths were adjusted to 750 nm and 900 nm for DAPI and Alexa Fluor 594, respectively. The data were reconstructed and analyzed with Imaris, version 9.0.1 (Bitplane AG, Zurich, Switzerland).

Hematoxylin and Eosin (H＆E) and immunostaining assays for FFPE sections

FFPE slides (thickness: 4 μm) were prepared from FFPE tissue blocks. Tissue sections were stained with H&E according to standard protocols. Immunohistochemical staining was performed according to the standard staining method including a routine deparaffinization and rehydration step, an acidic antigen retrieval step (20 minutes at 95˚C in Citric acid pH 6.0), an endogenous peroxidase quenching step (25 minutes at room temperature in 3% H_2O_2), and blocking with 3% BSA (Servicebio #G5001) for 30 minutes at RT. Primary antibodies (Lipopolysaccharide Core, clone WN1 222-5, HycultBiotech #HM6011, 1:1000 dilution; Lipoteichoic acid antibody，GeneTex #GTX16470，1:1000 dilution) were applied on slides overnight at 4˚C and secondary antibodies (HRP-conjugated Goat Anti-Mouse IgG, Servicebio #GB23301, 1:200 dilution) were added for 30 minutes at RT. The slides were covered with DAB chromogenic substrate (Servicebio #G1211) and the treating time was monitored under a Nikon E100 microscope (Nikon, Japan). Slides were counterstained with hematoxylin (Servicebio #G1004) for 3 minutes and routinely dehydrated with alcohol and xylene.

Slides were mounted with neutral balsam (SINOPHARM #10004160) and coverslips. Slides were scanned with Leica DM2500 Bright field microscope (Leica, Germany) at 40×.

16S RNA FISH for FFPE sections

The 4 μm FFPE tissue slides were routinely deparaffinized and hydrated. Slides were stained for bacterial 16S rRNA (Cy3 labeled EUB338 probes-GCTGCCTCCCGTAGGAGT, Future Biotech #FBFPC001, 25 μM) or negative control (Cy3 labeled nonspecific complement probe-CGACGGAGGGCATCCTCA, Future Biotech #FBFPC001, 25 μM) using the direct fluorescent bacteria in situ hybridization detection kit (Future Biotech #FB0016) according to the manufacturer's instructions. Briefly, slides were washed with 1×PBS (2×10 minutes, at RT) and then treated with HCl (0.2 N, 20 minutes) and Proteinase K (50 μg/mL, 20 minutes) at RT. Slides were washed with 1×PBS (1×5 minutes, at RT) and then incubated with 200μl blocking buffer for 2 hours at 55˚C. Slides were washed in PBS for 5 minutes and air-dried. The probe solutions (1:100 dilution, 250 nM) were prepared by mixing probes with 25% hybridization buffer and hybridized for 48 hours at 42˚C. Then slides were washed in pre-warmed washing buffer (37˚C) for 15 minutes and air-dried for 20 minutes. Finally, slides were mounted with 20 μl DAPI-Antifade solution for 10 minutes and covered with cover slides in dark. The slides were observed under confocal laser scanning microscopy (TCS SP8, Leica, Germany) equipped with ×63 objectives lens (HC PL APO CS2 63X/1.40 OIL).

Image processing

Laser power and gain values were adjusted to the optimum for each image so that the fluorescence of positive signals and cell nucleus can be displayed clearly. 3D image reconstruction was made with Imaris imaging software (version 9.0.1, Bitplane AG, Zurich, Switzerland). Subsequently, each fluorescence image was processed by MATLAB (version R2019b) for counting the objects and calculating the mean

fluorescence intensity and volume of each bacterial LPS fluorescent signal. In this process, we firstly binarized each slide along the depth in the Z-axis of one 3D image by a specific threshold, which was obtained based on the mean gray value of the slide, to roughly segment the bacterial signals. To further refine the segmentation, we conducted a region growing method for each object to make it include the surrounding pixels with high and close gray values. All the slides of one image were rearranged to screen the real bacterial objects with a diameter of 0.5~5 μm. The final statistics of bacteria load, objective sizes, and the mean fluorescence intensities were based on those screened bacterial LPS fluorescent signals. The MATLAB code is available at https://github.com/PRBioimages/Fluorescence-object-counting. It can be used for high-throughput automated processing of 3D fluorescence images.

Data availability

The data that support the findings of this study are available from the corresponding author upon reasonable request.

References

25. Moyes, R.B. Fluorescent staining of bacteria: viability and antibody labeling. *Curr Protoc Microbiol* **Appendix 3**, Appendix 3K (2009).
26. Lee, K. *et al.* Optimised tissue clearing minimises distortion and destruction during tissue delipidation. *Neuropathology and Applied Neurobiology* **47**, 441-453 (2020).
27. Treweek, J.B. *et al.* Whole-body tissue stabilization and selective extractions via tissue-hydrogel hybrids for high-resolution intact circuit mapping and phenotyping. *Nat Protoc* **10**, 1860-1896 (2015).

Acknowledgments

We would like to thank Ms.Yining Li and Mr. Yisi Liu for their contribution towards imaging data acquisition. We would also like to thank all staff at the Neurosurgery Center of Zhujiang Hospital of Southern Medical University, and the technical staff of the Clinical Biobank Center for their kind assistance. Finally, we thank all tissue donors and their families who have kindly donated their resected specimens to the Clinical

Biobank Center.

Author contributions

HS and HG jointly conceptualized the study. HS and ZJ designed the study. TW provided expertise and participated in the design of the experiments. DH, HS, HML, and YL developed the methodological approaches. HS, HG, and HZ provided the lab resources; HS, TW, DH, and ZJ interpreted the data; ZJ, HS, and DH drafted the manuscript. YL, YK, and LG acquired the patient samples and information. HD, ZJ, TL, YL, and JL performed the assay and acquired the data. JZ, HS, DH, TW, YX, and XY analyzed and curated the data. SH, TW, HML, and HZ revised the manuscript. All authors read and approved the final manuscript.

Funding

The research was supported by the National Natural Science Foundation of China (No. 61803196), Guangdong Basic and Applied Basic Research Foundation (2020A1515010038), the Pearl River S&T Nova Program of Guangzhou (201710010047), the Hong Kong Scholars Program (No. XJ2016055), the Presidential Foundation of Zhujiang Hospital of Southern Medical University (No. yzjj2018rc03). Special Funds for the Cultivation of Guangdong College Students' Scientific and Technological Innovation (pdjh2020b0119).

Competing interests

The authors report no competing interests.

Figure legends

Fig.1 3D quantitative imaging of bacterial LPS fluorescent signals in human glioma sample

(a) Schematic representation for the 3D quantitative imaging protocol based on tissue clearing. (b and c) Human glioma samples before and after tissue clearing, respectively. (d) 500 μm-thick sections of glioma tissues (Glioma $1^{\#}$) were immunolabeled with anti-LPS (red) antibodies and DAPI (blue) and cleared with the above protocol (Autofluorescence quenched by $CuSO_4$). The inner 100 μm-thick tissue was observed with MPLSM and scanned for 3D reconstruction. The 3D reconstruction images of the acquired Z-stack showed the sporadic distribution of the fluorescent signals among the whole tissue, located near the cell nucleus or in the intracellular space. Scale bars are shown in the pictures. (e) Examples of quantitative data of 3D images include the load and size (μm^3) of LPS fluorescent signals. Each object was screened and identified from the 3D images. Objects were counted according to the depth in Z-axis (shown in the left graph) and each of them was binned according to the proportional object volume (shown in the right graph).

Fig.2 Visualization of bacterial LPS and LTA in human glioma samples with histopathological staining of FFPE sections

(a to c) FFPE slices from 3 human gliomas, Glioma $1^{\#}$, Glioma $2^{\#}$, and Glioma $3^{\#}$, were stained with H&E, anti-LPS antibodies, and anti-LTA antibodies, respectively. Bacterial LPS positive staining was demonstrated in the glioma, while LTA staining demonstrated negative. (d) FFPE slices from mouse brain tissues were stained with antibodies against bacterial LPS and LTA as a negative control. (e) FFPE slices from mouse intestine tissues were also stained as above as a positive control. Scale bars, 50 μm.

Fig.3 Visualization of bacterial 16S rRNA in human glioma samples with FISH staining

(a) and (b) Representative results of the positive 16S rRNA FISH (red, with EUB338 probes) and DAPI (blue) staining of human glioma FFPE slices. The fluorescent signals mostly demonstrated nuclear localization or sparsely dispersed in the tumor. Samples did not fluoresce when stained with NON338, the control complement probe of EUB338. (c and d) The 16S rRNA FISH (red) and DAPI (blue) staining of the mouse brain and mouse intestine tissues, as negative and positive controls, respectively. Scale bar, 50 μm.

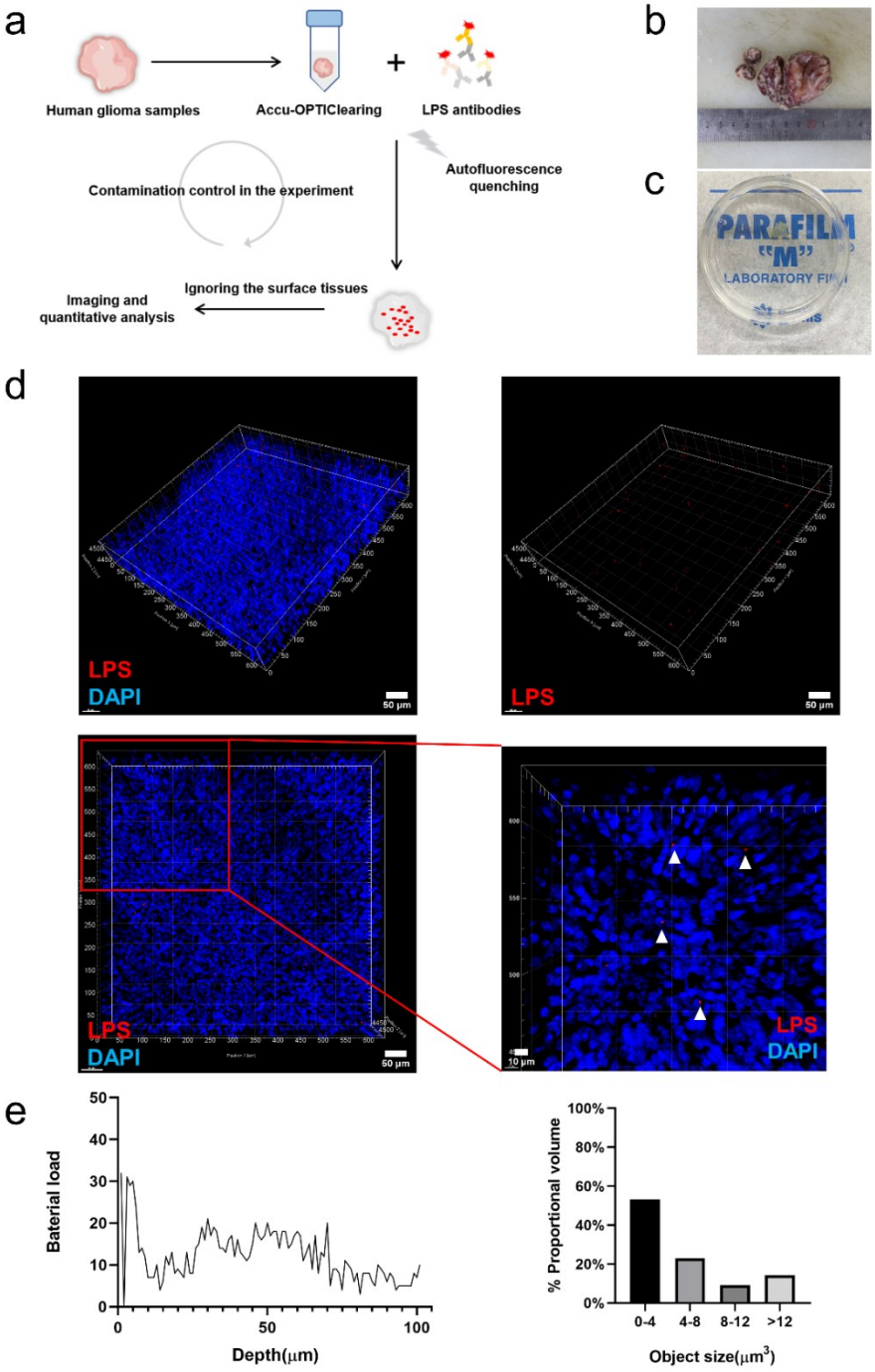

Fig.1 3D quantitative imaging of bacterial LPS fluorescent signals in human glioma sample

(a) Schematic representation for the 3D quantitative imaging protocol based on tissue clearing. (b and c) Human glioma samples before and after tissue clearing, respectively. (d) 500 μm-thick sections of glioma tissues (Glioma 1#) were immunolabeled with anti-LPS (red) antibodies and DAPI (blue) and cleared with the above protocol (Autofluorescence quenched by $CuSO_4$). The inner 100 μm-thick tissue was observed with MPLSM and scanned for 3D reconstruction. The 3D reconstruction images of the acquired Z-stack showed the sporadic distribution of the fluorescent signals among the whole tissue, located near the cell nucleus or in the intracellular space. Scale bars are shown in the pictures. (e) Examples of quantitative data of 3D images include the load and size (μm^3) of LPS fluorescent signals. Each object was screened and identified from the 3D images. Objects were counted according to the depth in Z-axis (shown in the left graph) and each of them was binned according to the proportional object volume (shown in the right graph).

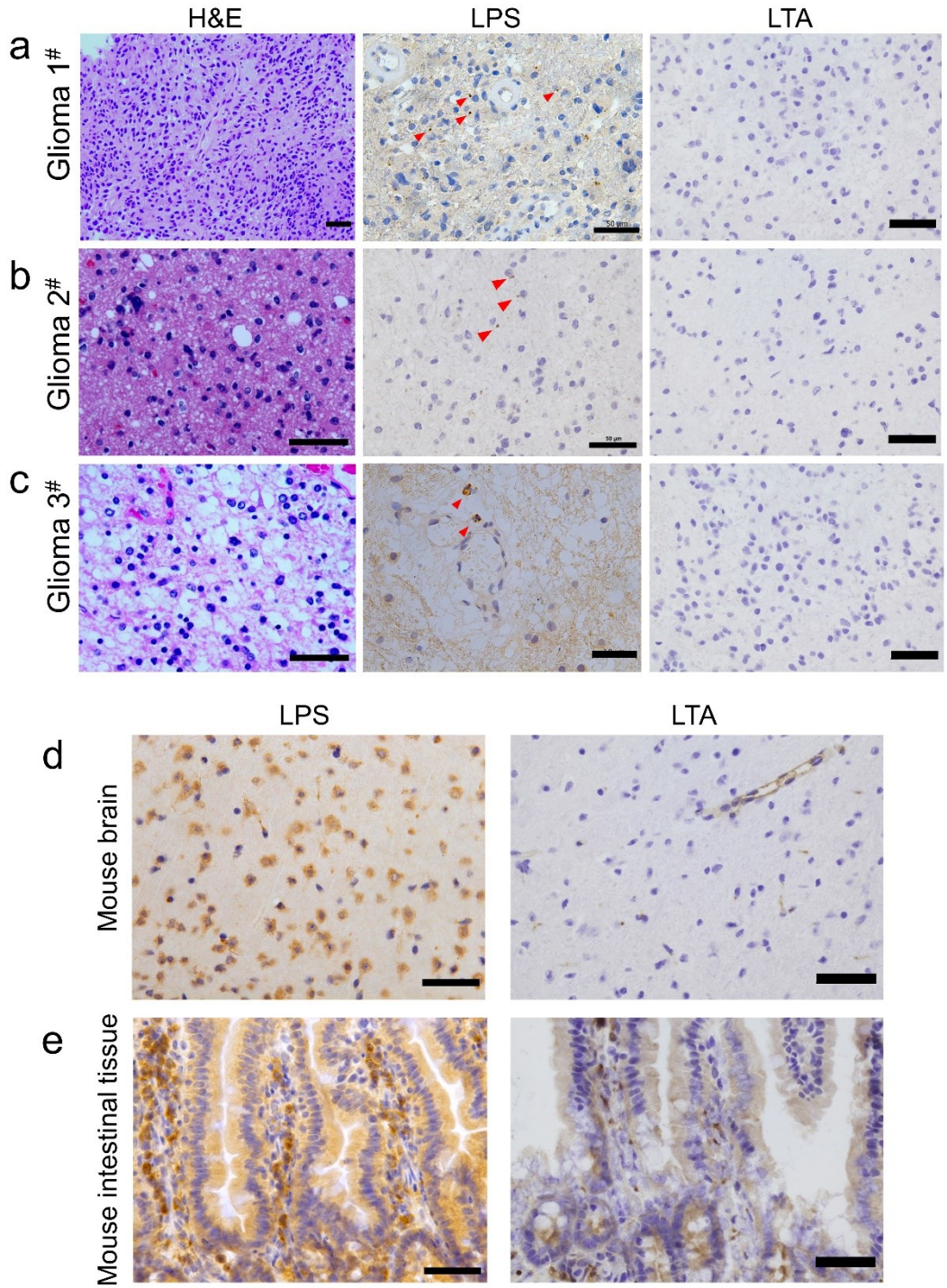

Fig.2 Visualization of bacterial LPS and LTA in human glioma samples with histopathological staining of FFPE sections

(a to c) FFPE slices from 3 human gliomas, Glioma 1#, Glioma 2#, and Glioma 3#, were stained with H&E, anti-LPS antibodies, and anti-LTA antibodies, respectively. Bacterial LPS positive staining was demonstrated in the glioma, while LTA staining demonstrated negative. (d) FFPE slices from mouse brain tissues were stained with antibodies against bacterial LPS and LTA as a negative control. (e) FFPE slices from mouse intestine tissues were also stained as above as a positive control. Scale bars, 50 μm.

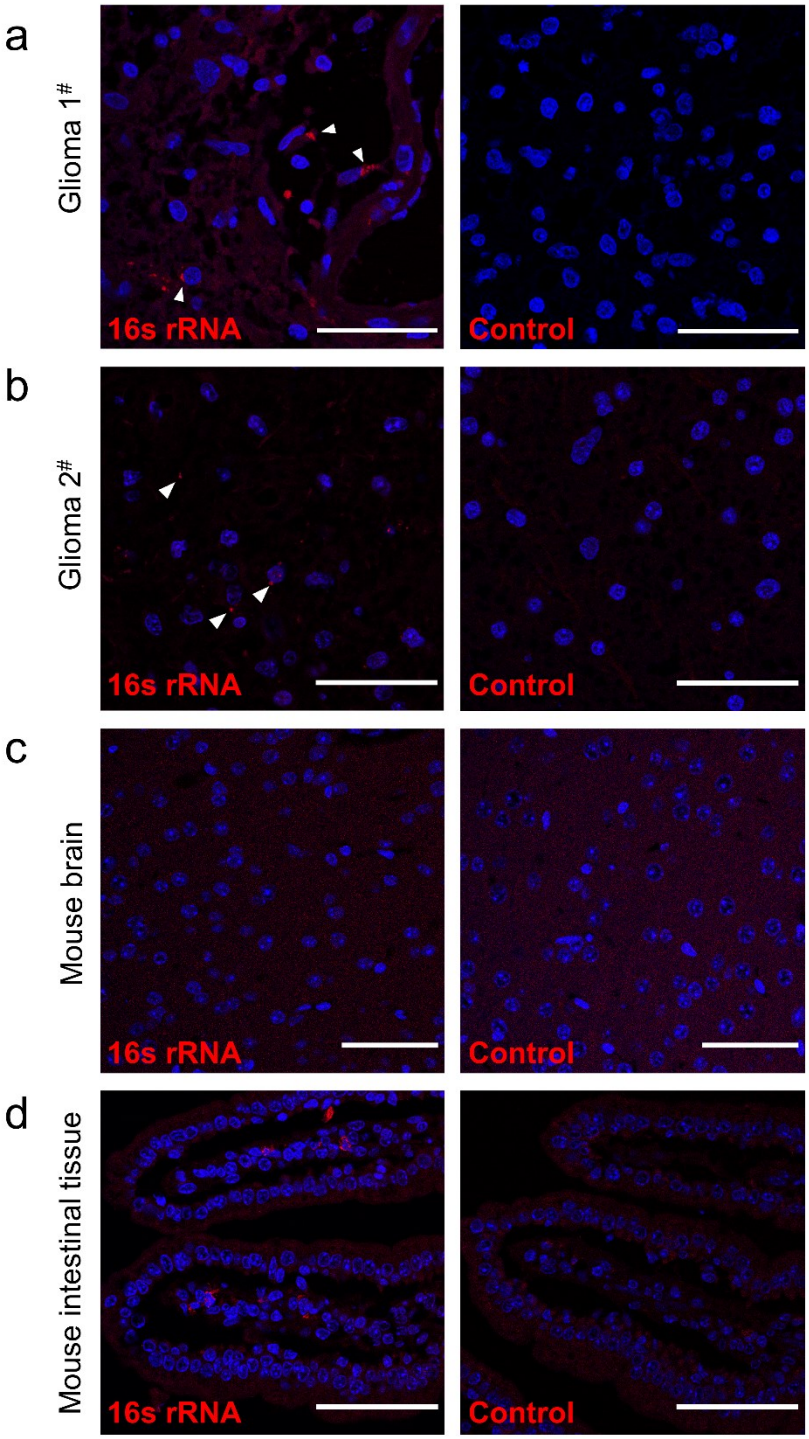

Fig.3 Visualization of bacterial 16S rRNA in human glioma samples with FISH staining

(a) and (b) Representative results of the positive 16S rRNA FISH (red, with EUB338 probes) and DAPI (blue) staining of human glioma FFPE slices. The fluorescent signals mostly demonstrated nuclear localization or sparsely dispersed in the tumor. Samples did not fluoresce when stained with NON338, the control complement probe of EUB338. (c and d) The 16S rRNA FISH (red) and DAPI (blue) staining of the mouse brain and mouse intestine tissues, as negative and positive controls, respectively. Scale bar, 50 μm.

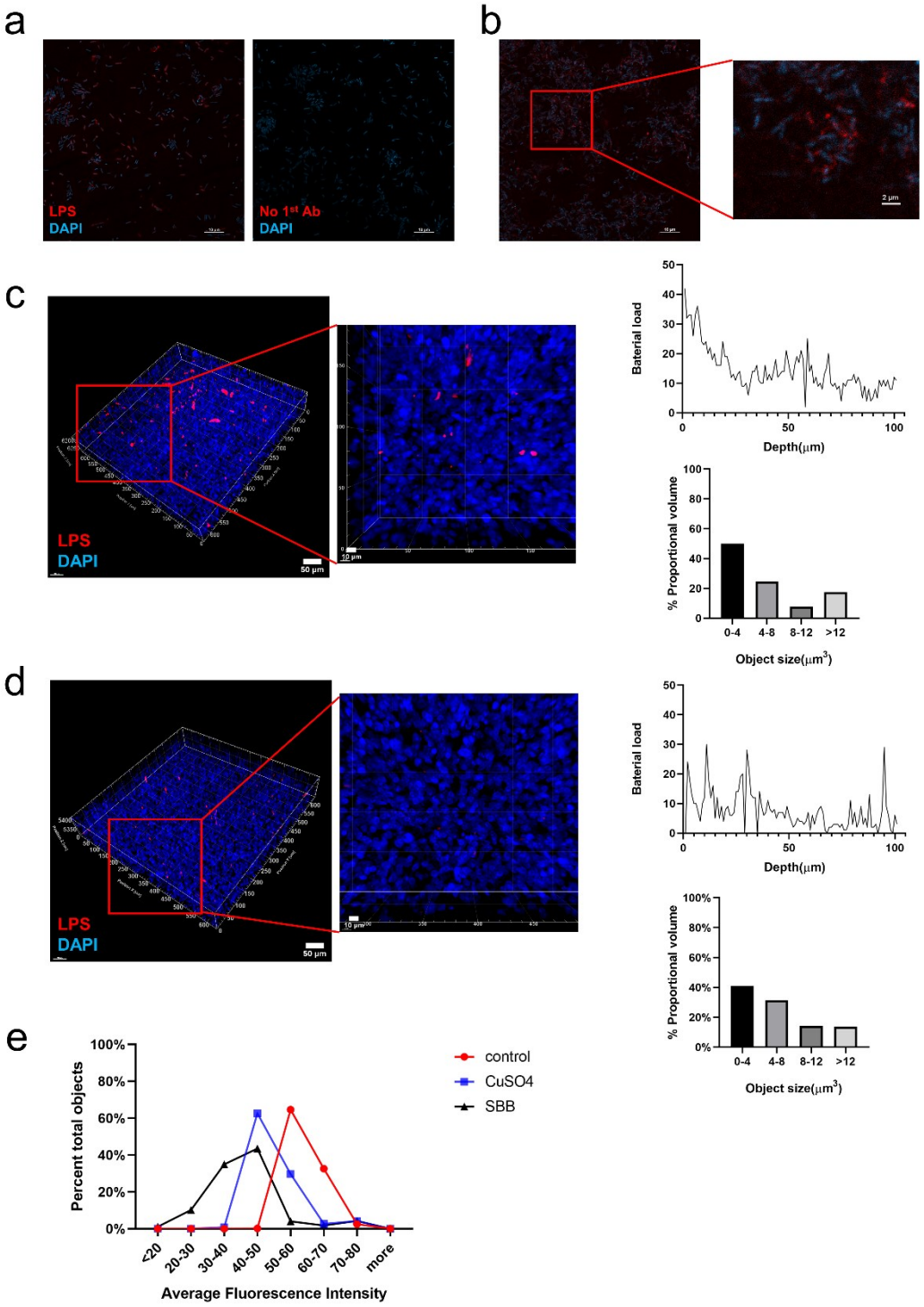

Extended Data Fig.1 | See next page for caption

Extended Data Fig.1 Results of LPS immunofluorescent labeling of E. coli and comparison of the results of visualization and quantitative analysis of bacterial LPS fluorescent signals within human glioma samples

(a) Specificity of LPS antibody. The bacteria smears of E.coli were immunolabeled with LPS primary antibody and secondary antibody, or without primary antibody as a control to exclude non-specific staining. Scale bar, 10μm. (b) Immunolabeling of LPS in bacteria smears, demonstrating incomplete attachment of antibodies and uneven staining pattern of fluorescence. Scale bars are shown in the pictures. (c) 3D quantitative imaging of bacterial LPS fluorescent signals in gliomas without an autofluorescence quenching step. The non-uniform shape, larger volume, and big quantity of the fluorescence signals in this group, compared with images after autofluorescence quenching (in **Fig.1** and **Extended Data Fig.1** d), indicated the presence of artifacts and false-positive results introduced by autofluorescence substances when performing the immunolabeling-based 3D histological imaging of thick tissues. (d) 3D quantitative imaging of bacterial LPS fluorescent signals with autofluorescence quenching step (with SBB). Scale bars are shown in the pictures. (e) The comparison of the mean fluorescence intensities of the three groups with/without autofluorescence quenching step (Control group has no autofluorescence quenching, in **Extended Data Fig.1** c; $CuSO_4$ group, in **Fig.1**; SBB group, in **Extended Data Fig.1** d). The average fluorescence intensity reduced in groups with the AF quenching step was shown in the graph.

Supplementary Files

This is a list of supplementary files associated with this preprint. Click to download.

- SupplementaryMovieS1.mov
- SupplementaryMovieS2.mov
- Supplementaryinformation.docx